Colloids and Surfaces B: Biointerfaces 100 (2012) 177–184

Contents lists available at SciVerse ScienceDirect

Colloids and Surfaces B: Biointerfaces

journal homepage: www.elsevier.com/locate/colsurfb

A systematic study of transfection efficiency and cytotoxicity in HeLa cells using iron oxide nanoparticles prepared with organic and inorganic bases

Marilia Freitas Calmon[a,1], Aryane Tofanello de Souza[b,1], Natalia Maria Candido[a,1], Maria Irene Bartolomeu Raposo[c], Sebastião Taboga[a], Paula Rahal[a,**], Jose G. Nery[b,*]

[a] Departament of Biology, São Paulo State University, São José do Rio Preto, São Paulo, Brazil
[b] Departament of Physics, São Paulo State University, São José do Rio Preto, São Paulo, Brazil
[c] Institute of Geosciences, University of São Paulo, São Paulo, Brazil

ARTICLE INFO

Article history:
Received 27 March 2012
Accepted 15 May 2012
Available online 30 May 2012

Keywords:
Iron oxide nanoparticles
Inorganic base
Organic bases
HeLa cells
Transfection efficiency
Toxicity

ABSTRACT

Magnetic iron oxide nanoparticles (magnetite) (MNPs) were prepared using different organic and inorganic bases. Strong inorganic base (KOH) and organic bases (NH_4OH and 1,4-diazabicyclo[2.2.2]octane (DABCO)) were used in the syntheses of the MNPs. The MNPs were characterized by X-ray diffraction (XRD), scanning electron microscope (SEM), Fourier transform infrared spectroscopy (FT-IR) and magnetization measurements. MNPs prepared with strong inorganic base yielded an average size of 100 nm, whereas the average size of the MNPs prepared with the organic bases was 150 nm. The main competitive phase for MNPs prepared with the strong inorganic and organic bases was maghemite; however, syntheses with KOH yielded a pure magnetite phase. The transfection study performed with the MNPs revealed that the highest transfection rate was obtained with the MNPs prepared with KOH (74%). The correlation between the magnetic parameters and the transfection ratio without transfection agents indicated that MNPs prepared with KOH were a better vector for possible applications of these MNPs in biomedicine. HeLa cells incubated with MNP-KOH at 10 μg/mL for 24 and 48 h exhibited a decrease in population in comparison with the control cells and it was presumably related to the toxicity of the MNPs. However, the cells incubated with MNP-KOH at 50 and 100 μg/mL presented a very small difference in the viability between the cell populations studied at 24 and 48 h. These data illustrate the viability of HeLa cells treated with MNP-KOH and suggest the potential use of these MNPs in biomedical applications.

1. Introduction

Nanotechnology, which is based upon the systematic organization, fabrication or manipulation of matter on the nanometer scale, has triggered a scientific and technological revolution because it allows unique and distinctive material properties to be attained [1]. Due to their intrinsic magnetic properties and connections to biological systems, magnetic nanoparticles have generated significant interest in the field of biomedical and clinical applications. In particular, studies of such nanoparticles frequently examine their functions in cell labeling, cell separation, magnetofection, targeted drug delivery, induction of local hyperthermia and magnetic resonance imaging (MRI) [2].

Studies of cell labeling, cell tracking and homing are crucial for understanding the role of the nanoparticles in cell therapeutics. An understanding of these mechanisms will augment the benefit of therapeutic approaches by enabling cells to be tailored appropriately for specific situations [3]. However, transfection agents are needed to achieve the intracellular uptake of nanoparticles in certain cell lines [4,5,6]. Several of the most commonly used transfection agents are positively charged, whereas magnetic nanoparticles are negatively charged; thus, transfection agent usage can result in the loss of the nanoparticle surface charge, causing nanoparticle precipitation. In addition, transfection agent usage can result in nanoparticle adsorption to the cell surface rather than the internalization of the nanoparticles [4]. Thus, avoiding a transfection agent in the process of cell labeling appears to be desirable for the reasons described above.

Laurent et al. have described the influence of several parameters, such as pH, ionic strength and temperature, on the formation and

* Corresponding author at: Departamento de Física, Instituto de Biociências, Letras e Ciências Exatas, UNESP – Universidade Estadual Paulista, Campus de São José do Rio Preto, São Paulo 15054-000, Brazil. Tel.: +55 17 3221 2490; fax: +55 17 3221 2247.
** Corresponding author at: Departamento de Biologia, Instituto de Biociências, Letras e Ciências Exatas, UNESP – Universidade Estadual Paulista, Campus de São José do Rio Preto, São Paulo 15054-000, Brazil. Tel.: +55 17 3221 2379; fax: +55 17 3221 2347.
E-mail addresses: rahalp@yahoo.com.br (P. Rahal), nery@ibilce.unesp.br (J.G. Nery).
[1] All the three authors equally contributed to this work.

0927-7765/$ – see front matter © 2012 Elsevier B.V. All rights reserved.
http://dx.doi.org/10.1016/j.colsurfb.2012.05.026

properties of magnetic magnetite nanoparticles [2]. The yield of the coprecipitation reaction, the nanoparticle diameter and the polydispersity of the iron MNPs can be affected by the base used, and the effects of several organic anions, such as carboxylate and hydroxy carboxylate ions, on the formation of iron oxides or oxyhydroxides have been studied extensively in the syntheses of magnetic nanoparticles [7–9]. There are few studies with KOH and other less common organic bases. In this study, we explored this reaction, using KOH and 1,4-diazabicyclo[2.2.2]octane (DABCO) to synthesize MNPs. DABCO has also been used as an organic base and structure-directing agent in the syntheses of microporous materials, such as zeolites [10].

In this study, uncoated MNPs were synthesized with KOH (MNP-KOH), NH_4OH (MNP-NH_4OH) and DABCO (MNP-DABCO), and attempts were made to transfect these MNP variants into a HeLa cell line without the use of a transfection agent. We used the HeLa cell line to perform the transfection of MNPs because HeLa cells are a cervical cancer cell line that has been widely used for investigating cancer biology and that is recognized for its immortal behavior owing to telomerase activity [11]. To the best of our knowledge, this report is the first that describes a cancer cell line labeled with even a low concentration (10 μg/mL) of MNPs synthesized with KOH. Moreover, an increase in cytotoxicity was not observed, even after a long incubation period of MNPs in HeLa cells.

2. Materials and methods

2.1. Synthesis of DABCO derivatives

The DABCO derivative was synthesized according to the following procedure: 80 g of 1,4-diazabicyclo[2.2.2] octane (DABCO) was dissolved in 100 mL methanol and placed into a round-bottomed liter flask equipped with a magnetic stirring bar, reflux-condenser, thermometer and funnel. A total of 77.4 grams of 1,4-dibromobutane was added to the flask at a rate that maintained the reaction temperature at 50 °C. After the addition of the 1,4-dibromobutane, the mixture was stirred at room temperature for 2 h. Then, 300 mL of dry diethyl ether was added to the flask, and the solid product DABCO-C_4-diquat bromide was filtered off the reaction mixture. The aforementioned halides were anion-exchanged into their hydroxide form using anion-exchange resin. A typical procedure for anion exchange was conducted as follows: AG1-X8 OH (Bio-Rad) anion-exchange resin was added to a solution of DaB-A-bromide (5 g, 20 mmol) in water and the mixture was stirred at room temperature for 24 h. After filtration, the aqueous solution was concentrated to a volume of approximately 25 mL to produce 0.75 mmol/g of DaB-A-hydroxide, based on a titration of the resultant solution. This solution was used in the synthesis of the magnetic nanoparticle.

2.2. Synthesis of magnetic nanoparticles using NH_4OH, KOH and DABCO

A typical synthesis of magnetic nanoparticles, independent of the base used, is described as follows: Fe_3O_4 magnetic nanoparticles were prepared by the chemical co-precipitation method using a strong inorganic base (KOH) and a weak organic base (NH_4OH). Reagents such as iron (III) chloride hexahydrate ($FeCl_3{\cdot}6H_2O$, Merck, 99%), iron (II) sulfate heptahydrate ($FeSO_4{\cdot}7H_2O$, Sigma–Aldrich, 99%), ammonium hydroxide sol (NH_4OH, Sigma–Aldrich, 28–30% of ammonia) and anhydrous citric acid (Sigma–Aldrich ≥99.5%) were used for the synthesis. A solution of 0.023 M ferric chloride was added to a 0.027 M ferrous sulfate solution, which was stirred for 15 min under an atmosphere of N_2. The salts were mixed and kept at room temperature while maintaining a molar ratio of Fe^{2+}/Fe^{3+} of 1/2. Subsequently, a solution of ammonium hydroxide (NH_4OH, 8 M) was added (pH between 10 and 11.8), and a black precipitate was formed immediately. The mixture was stirred for 30 min at 800 rpm using magnetic agitation. To avoid the agglomeration of the nanoparticles, approximately 50 mL of an aqueous solution of 0.02 g/mL citric acid was added, and the mixture was incubated at 80 °C for another 60 min. Finally, the product was decanted, washed three times and dried at 40 °C for several hours. The syntheses using other bases were conducted in the same matter, although with several slight adjustments to the general stoichiometric ratio of $Fe^{2+}{:}2Fe^{3+}{:}8OH^-$.

2.3. Characterization of the nanoparticles

The X-ray diffraction (XRD) patterns of the MNPs were collected with a Rigaku Rota Flex on a rotating anode source, using a flat-plate Bragg–Brentano geometry, operating with Cu Kα radiation (λ = 1.5418 Å), 50 kV, 100 mA and equipped with a graphite monochromator. The powder diffraction patterns were recorded in the range of $2\theta = 5–80^\circ$, with a step scan of 0.02°, and at a rate of 10 s/step. The crystal size was calculated from the X-ray line broadening analysis using the Debye–Scherrer equation, $D = 0.9\lambda/\beta\cos\Theta$, where D is the crystal size in nm, and λ is the X-ray wavelength. β is the half-width of the peak in rad, and Θ is the corresponding diffraction angle. Fourier transform infrared (FT-IR) spectra were recorded on a Nicolet 380 spectrometer with the standard KBr pellet method. The morphology of the nanoparticles was observed by scanning electronic microscopy (SEM). The SEM images were recorded using an XL30 FEG instrument, and before the analysis, a thin gold sputter coating was deposited onto the samples. The magnetic properties of the nanoparticles were measured at room temperature using a vibrating sample magnetometer (VSM-Nuvo, Molspin) in a magnetic field applied up to 1 T. The potential Zeta of the samples was measured to determine the surface properties using a Malvern Zeta Master. The samples were prepared in various buffered pH solutions and in the appropriate cell medium.

2.4. Cell line and nanoparticles treatment

HeLa cells were purchased from the American Type Culture Collection (ATCC). The cells were cultured in Dulbecco's Modified Eagle Medium (DMEM) (Gibco) supplemented with 10% heat-inactivated fetal bovine serum (FBS), penicillin (50 U/mL) and streptomycin (0.05 mg/mL). The cells were incubated at 37 °C with 5% CO_2. For the incubation with MNPs, MNP-KOH, MNP-NH_4OH and MNP-DABCO were added to the culture medium at concentrations of 10, 50 and 100 μg MNP/mL. To avoid contamination in the cell culture, filter sterilization (using a Millipore filter with a pore size of 220 μm) of the DMEM containing the MNPs was applied before introducing the medium to the cell culture.

2.5. Prussian blue staining

Cells were suspended in a chambered cover glass at a density of 2×10^5 cells/mL. Medium containing MNPs at concentrations of 10, 50 or 100 μg MNP/mL was added. The cells were incubated with the MNPs for 24 h and were washed repeatedly to remove unbound particles. The cells were then fixed using 2 mL of Karnovsky's solution (4% paraformaldehyde:4% glutaraldehyde) for 1 h, washed with distilled water, and treated with a 1:1 mixture of 4% potassium ferrocyanide and 4% HCl for 20 min at RT. Upon completion, the slides were rinsed three times with distilled water, treated with hematoxylin for 10 min, incubated at room temperature (RT) with distilled water for 10 min, rinsed with alcohol and treated with eosin as a counterstain for 4 min. This was followed by one last rinse with distilled water. The resulting slides were observed under 400×

magnification with an Olympus BX60 light microscope. To analyze the transfection efficiency of the MNPs, 500 cells were counted in different fields under the same magnification, and the cells labeled with MNPs were quantified. Each experiment was performed in triplicates and in two independent assays.

2.6. Apoptosis assay

HeLa cells were suspended in a chambered cover glass at a density of 2×10^5 cells/mL. Medium containing MNPs at concentrations of 10, 50 or 100 μg MNP/mL was added. The cells were incubated with the MNPs for 24 h, then fixed with 2 mL of Karnovsky's solution (4% paraformaldehyde:4% glutaraldehyde) for 1 h and washed with distilled water. Subsequently, 2 mL of 4% ferric alum was added for 4 min, the solution was removed, and the slides were rinsed with distilled water and treated with acridine orange as a counterstain for 10 min. The resulting slides were observed under 400× magnification with an Olympus BX60 light microscope. Each experiment was performed in triplicates and in two independent assays.

2.7. MTT assay

The cytotoxicity was assessed using the MTT assay, which is a nonradioactive colorimetric assay. Medium containing MNPs at concentrations of 10, 50 or 100 μg/mL was added to each well containing cells at the density of 1×10^4 cells. After 24 and 48 h of incubation with the MNPs, 10 μL of MTT (5 mg/mL) (Invitrogen) was added to 100 μL of medium in each well. Following 4 h of incubation, the medium was removed and the formazan crystals were solubilized by incubating for 10 min in 50 μL of DMSO (Sigma). The absorbance of each well, which identifies the quantity of viable cells, was read at 570 nm on a microplate reader (Thermoplate model TP reader type B). Each experiment was performed in triplicates and in three independent assays.

2.8. Statistical analysis

In the present MTT assay studies, all of the experiments were conducted at least in triplicate and the results expressed as (mean ± standard deviation). The standard deviation values are indicated as error bars in the subsequent MTT graphs. The results were statistically processed for outlier detection, using a so-called "T procedure" in the MINITAB software (Minitab Inc.). Statistical judgments were determined by a one-way analysis of variances (ANOVA), during which a probability of $p < 0.05$ was considered to be statistically significant for a value being an outlier.

3. Results and discussion

3.1. Characterization of the magnetic nanoparticles

The XRD patterns (Fig. 1) of the MNPs synthesized with KOH and NH_4OH were basically the same. Both XRDs were characterized by the typical reflections (2 2 0), (3 1 1), (4 0 0), (4 2 2), (5 1 1) and (5 3 3). Those reflections are the fingerprints of the spinel structure, which is the structure of the MNPs, and they are in accordance with the data reported in the literature [2]. However, although the DABCO molecules were able to direct the synthesis of the MNPs, there is a significant difference at the region 2θ (5–10°). We attempted to characterize this phase in comparison with several of the most common competitive phases that occur in the synthesis of MNPs, such as maghemite, hematite or goethite [2]; however, none of these phases could be assigned to this broadened diffraction peak. It is possible that the peak is related to the formation of a non-magnetic amorphous hydroxide, which is very common in the complex synthesis system of magnetic nanoparticles with spinel

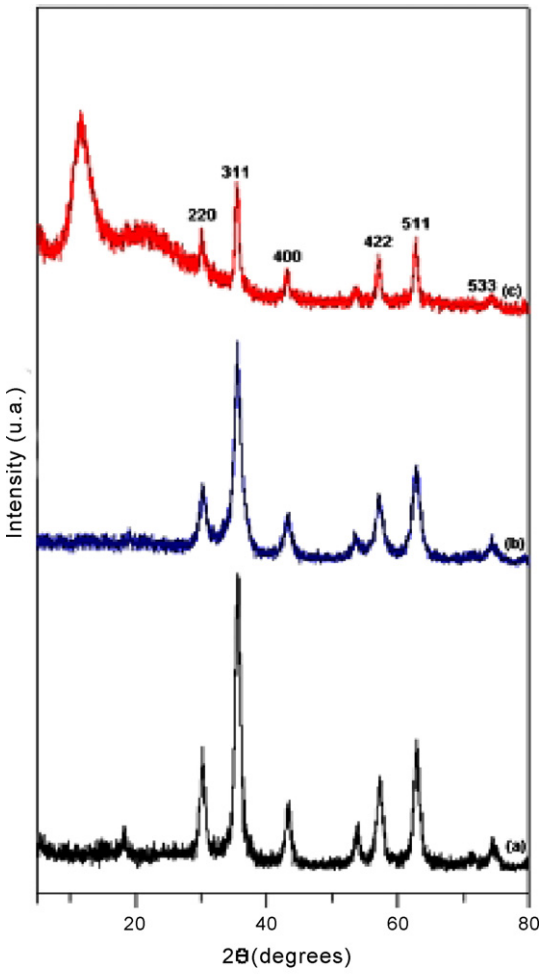

Fig. 1. XRD of the MNPs: (a) MNP-KOH, (b) MNP-NH4OH, (c) MNP-DABCO.

structure, such as the oxyhydroxide competitive phases present during the formation of Co_3O_4 [12].

The average crystal size of the MNPs (89 nm) was calculated using the Debye–Scherrer formula on the (3 1 1) XRD peaks of the spectrum, which is largely consistent with the scanning electron microscopy. The SEM data (Fig. 2) revealed that the different type of base did not influence the morphology of the MNPs. All of the MNPs were characterized by a spherical form and a mean size of 90 nm, which is consistent with the size calculated using the Debye–Scherrer formula.

The FT-IR spectra (not shown) presented vibration bands with peaks at 587.1 and 457.57 cm^{-1} that can be assigned to the stretching modes of Fe—O, and the other two vibrations (1630.30 and 3421.18 cm^{-1}) were due to the stretching vibration of —OH and the bending vibration of the H_2O molecules.

The magnetic properties of the MNPs were measured at room temperature using a vibrating sample magnetometer (VSM-Nuvo, Molspin, Newcastle-upon-Tyne, UK) in a magnetic field applied up to 1 T. The hysteresis loop was made to determine the specific saturation magnetization (M_s) and coercivity (H_c) (Fig. 3). According to the literature, the magnetic saturation values of MNPs were experimentally determined to be in the range of 30–50 emu g^{-1}, which is lower than the bulk value, 90 emu g^{-1} [2]. Our data indicated that the M_s values for MNP-KOH, MNP-NH_4OH and MNP-DABCO were estimated to be 73.8, 51.6, and 4.70 emu g^{-1} respectively. The low M_s observed for the MNPs prepared with DABCO can be associated with the low crystallinity of this sample, as shown in the XRD data

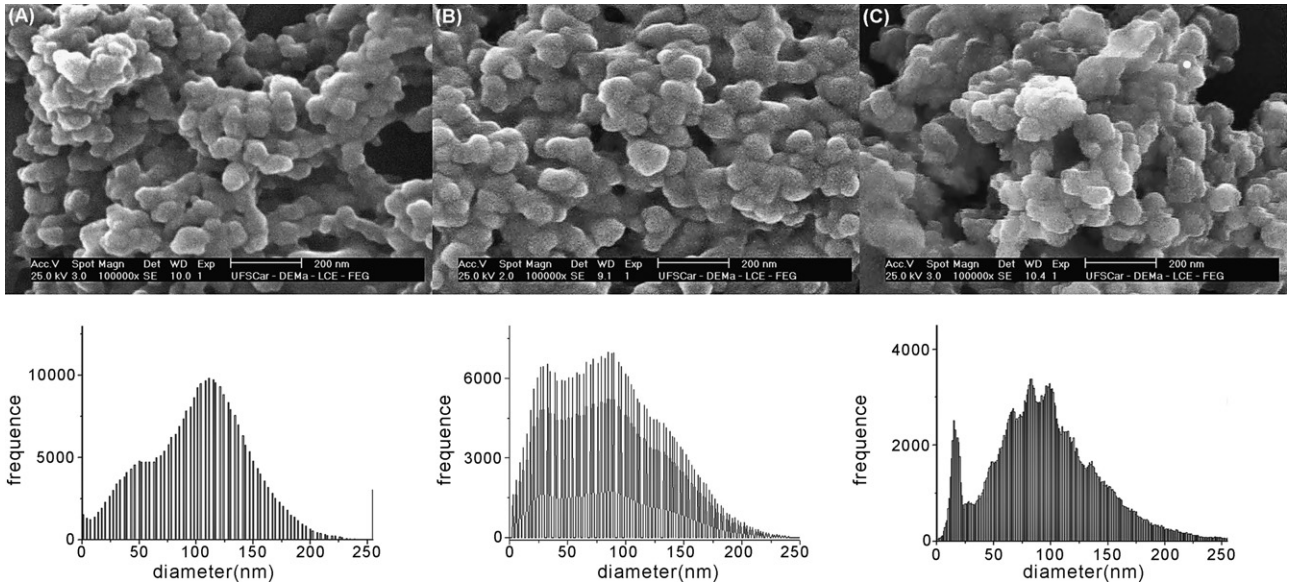

Fig. 2. SEM and size distribution of the MNPs: (A) MNP-KOH, (B) MNP-NH4OH, (C) MNP-DABCO.

(Fig.e 1c). The remanence (M_r) and coercivity (H_c) values for MNP-KOH (0, 0.25), MNP-NH_4OH (0.5, 0.24), and MNP-DABCO (0.01, 0.0) were also determined. Although these values were not null, they were very low, which is an indication of the superparamagnetic nature of the materials. This result indicates that the magnetic materials can be aligned under an external magnetic field but that they will not retain any residual magnetism when the external field is removed.

To understand the interaction of the MNPs with the cell medium, the Zeta potentials for MNPs were measured, both in aqueous solution and in the cell medium (DMEM). The values of the Zeta potential in aqueous solution were different for each MNP: MNP-KOH (−65.0 mV), MNP-NH_4OH (+28.9 mV) and MNP-DABCO (−30.1 mV). By contrast, in the cell medium, the values were similar: MNP-KOH (−15.4 mV), MNP-NH_4OH (−18.5 mV) and MNP-DABCO (−15.8 mV). These results indicated that the MNPs were stabilized by the cell medium and, in principle, were subjected to the same encapsulation process by the HeLa cell membranes.

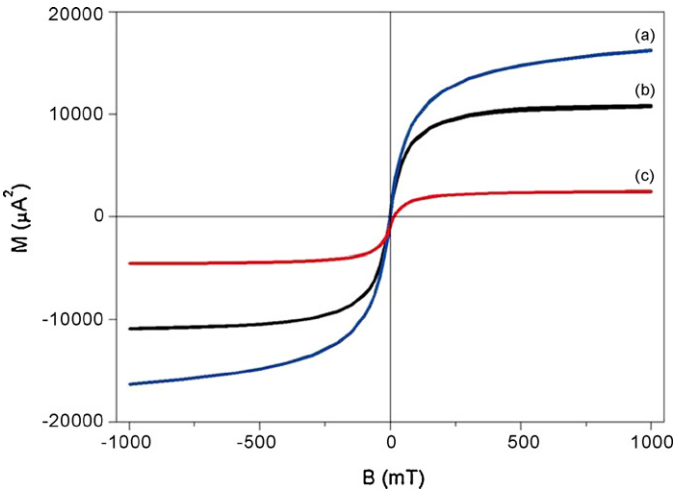

Fig. 3. Hysteresis loop of the magnetic nanoparticles at room temperature. (a) MNP-KOH, (b) MNP-NH4OH, (c) MNP-DABCO.

3.2. Prussian blue staining

After the physical and chemical characterization of the MNPs, we assessed whether these MNPs could label HeLa cells by passive MNP uptake without the use of transfection agents. For quantification of the uptake of uncoated MNPs into the cells, HeLa cells incubated with 10, 50 and 100 μg/mL of these MNPs were further qualitatively analyzed for their iron content. No stainable iron was detected in the non-transfected HeLa cells (experimental control). HeLa cells incubated with MNP-NH_4OH and MNP-DABCO presented a low percentage of cells labeled, independent of the MNPs concentrations. In contrast to MNP-NH_4OH and MNP-DABCO, which were able to transfer only a very small amount of nanoparticles inside the cells, MNP-KOH displayed a completely different behavior. This MNP exhibited a labeling efficiency of 44.1% in HeLa cells transfected with 10 μg/mL, 50% in cells transfected with 50 μg/mL and 74% in cells transfected with 100 μg/mL of MNP-KOH (Fig. 4).

HeLa cells incubated without MNP-KOH (experimental control) and incubated with MNP-KOH at 10 μg/mL and 50 μg/mL presented a normal rate of cell growth and unaltered cell morphology (Fig. 5A–E). It was also observed that cells labeled with MNP-KOH underwent mitosis with the division of the MNPs between

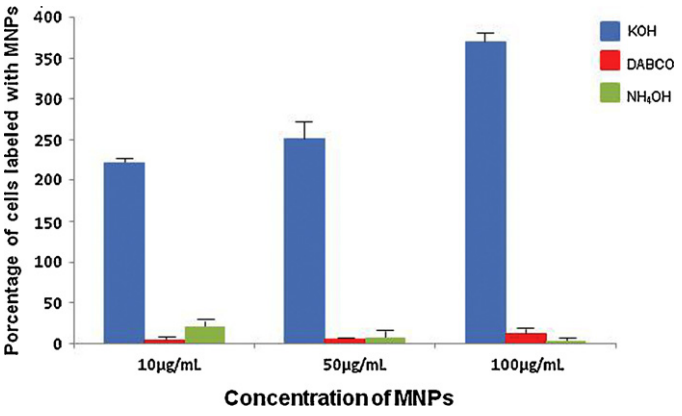

Fig. 4. Efficiency of cell labeling by three different MNPs.

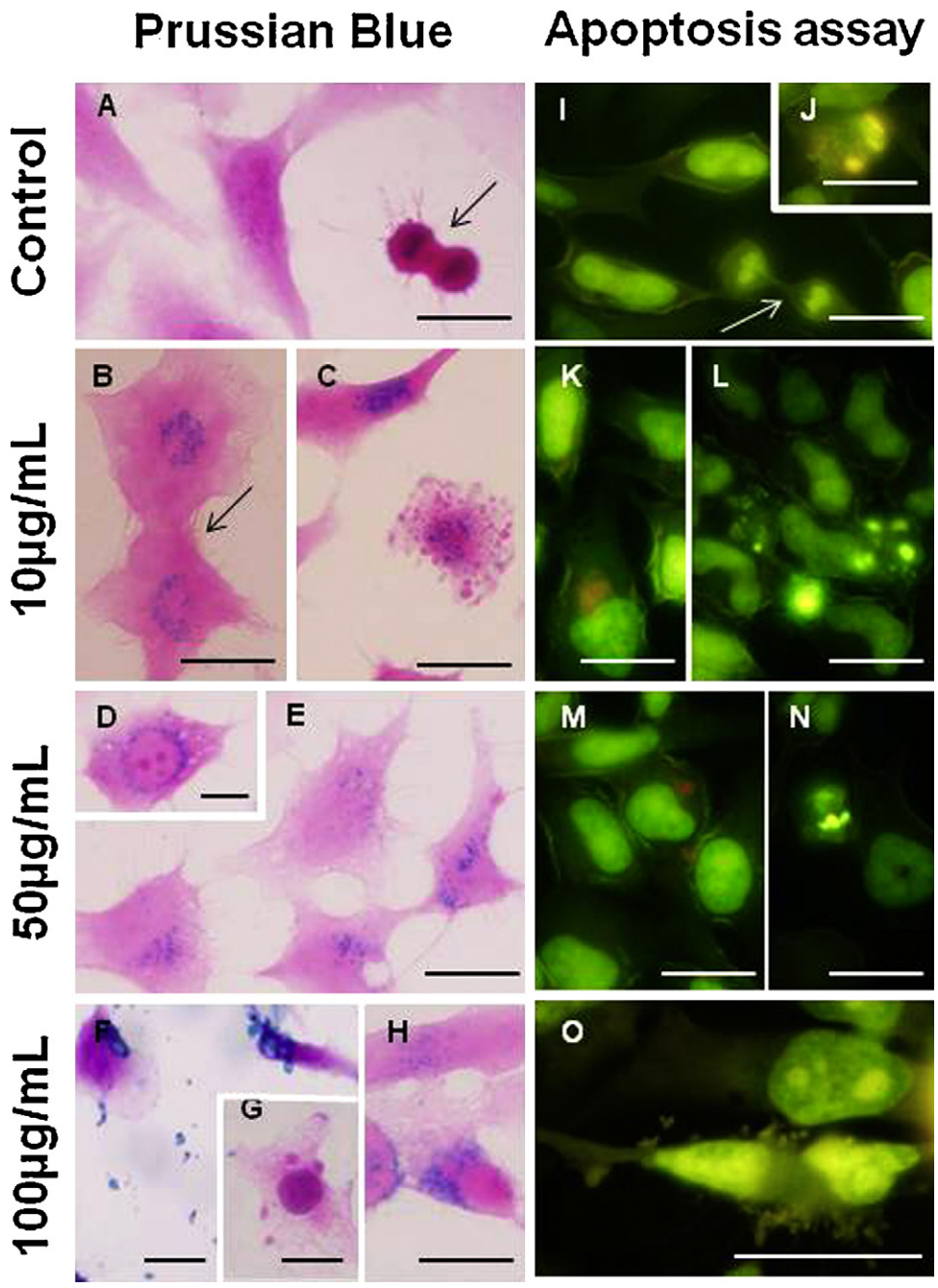

Fig. 5. Prussian blue staining and apoptosis assay: in the Prussian blue staining, MNPs are blue-stained. (A) A control experiment without MNPs. (B) and (C) Cells incubated with MNP-KOH at 10 μg/mL. (D) and (E) Cells incubated with MNP-KOH at 50 μg/mL. (F), (G) and (H) Cells incubated with MNP-KOH at 100 μg/mL. In the apoptosis assay, the fluorescent green cells are live cells, and the orange-red cells are cells undergoing apoptosis. (I) and (J) A control experiment without MNPs. (K) and (L) Cells incubated with MNP-KOH at 10 μg/mL. (M) and (N) Cells incubated with MNP-KOH at 50 μg/mL. (O) Cells incubated with MNP-KOH at 100 μg/mL. The arrows indicate cells in the process of mitosis.

the daughter cells (Fig. 5B). Serda et al. [13] and Sirimuthu et al. [14] also observed this phenomenon in endothelial cells and in Chinese Hamster ovary cells (CHO) respectively. In their study, it was observed that after mitosis, each daughter cell contained a similar amount of nanoparticles, providing support for a highly ordered process leading to the equal partitioning of endosomes during mitosis.

The amount of MNPs that was not endocytosed and remained in the cell medium was much higher for the MNP-KOH at 100 μg/mL (Fig. 5F). It was observed that the capacity for cell absorption was exceeded at 100 μg/mL, as the visible amount of MNP-KOH staining outside the cell was much higher compared with the cell absorption patterns observed in 10 and 50 μg/mL.

As reported in the literature, extracellular aggregation of the incubated nanoparticles is quite normal in cellular media containing bovine serum [15]. These conglomerates cannot be easily washed away, as they adhere to the cell surfaces. We also have observed large aggregates of MNPs outside the cells, which is an indication of their interaction with the cellular medium (Fig. 5F).

In our study, we observed the formation of vesicles in HeLa cells transfected with MNP-KOH at 100 μg/mL (Fig. 5G). Mahmoudi et al. have also observed similar phenomena in their study with mouse

Table 1
Zeta potential and conductivity of MNPs in cell medium and water.

	Samples	Cell medium (DMEM)	Water
Zeta potential	KOH	−15.4 ± 2.9 mV	−65.9 ± 1.3 mV
Conductivity		17.5 mS/cm	0.23 mS/cm
Zeta potential	NH_4OH	−18.5 ± 1.4 mV	+28.9 ± 1.3 mV
Conductivity		17.5 mS/cm	0.0306 mS/cm
Zeta potential	DABCO	−15.8 ± 0.5 mV	−30.1 ± 0.7 mV
Conductivity		17.4 mS/cm	0.024 mS/cm

fibroblasts cells transfected with higher concentrations of SPIONs, which resulted in the formation of bubbles [16]. One plausible explanation they raised was the correlation between the toxicity of the SPIONs and their interactions with the proteins and the medium, changing their functions and changing the ionic equilibrium.

One possible way to explain the encapsulation of the nanoparticles by the cells is to correlate the surface charge of the nanoparticles and the charge of the cell membranes. In general, the surface charges of the nanoparticles are negative due to their interaction with the OH groups of the water molecules, and these surfaces charges give rise to an electric field that attracts counter ions. The interaction of the nanoparticles and cell membrane proteins is very complex, and the encapsulation process can be described by two main mechanisms: phagocytosis and pinocytosis [1]. Among the several factors that can influence these two possible mechanisms, the surface charge of the nanoparticles is one of them. The nanoparticles' surface charges can be modified by the cell medium. Mahamoudi et al. have observed that coated nanoparticles presented positive surface charges in the presence (+10.2 mV) or absence (+3.21 mV) of serum in the cell medium (DMEM). However, for uncoated nanoparticles, the values were (+16.32 mV) and (−21.4 mV) in the presence and absence of serum, respectively [16]. Our results show a completely different behavior, as all of the MNPs in the presence of the cell medium (DMEM) presented a negative surface charge. Table 1 shows the surface charge of the MNPs in the presence and absence of the cell medium, and it is worth noting that all of the MNPs presented a negative surface charge in the presence of the cell medium, which is quite different from other results reported in the literature [16].

Based on our Zeta potential data and particle size measurements, we believe that the MNPs in our system were encapsulated via pinocytosis (adsorptive endocytosis) through a nonspecific adsorption onto the membranes of the cancer cells (HeLa) through electrostatic interactions [17]. As reported in the literature, when plasma membrane cationic sites (HeLa cells) are much scarcer than anionic sites, the adsorbed anionic nanoparticles are inferred to form clusters due to repulsive interactions with the large negatively charged domains. We have observed the formation of these clusters in our experiments (Fig. 5H). Wilhem et al. have explained that the formation of these clusters is due the repulsive interactions of the negatively charged nanoparticles with the negatively charged domains of the cell surface; therefore, the high efficiency of cell uptake of anionic particles is related, first, to the non-specific process of nanoparticle adsorption onto the cell membrane and second, to the formation of nanoparticle clusters [17].

3.3. Apoptosis assay

Due to the low transfection degree observed in HeLa cells incubated with MNP-NH_4OH and MNP-DABCO, apoptosis and MTT assays were performed only with cells incubated with MNP-KOH. In this case, morphological changes characteristic of apoptotic cells were observed, such as cell rounding, bubble formation on the membrane and nuclear fragmentation into apoptotic bodies.

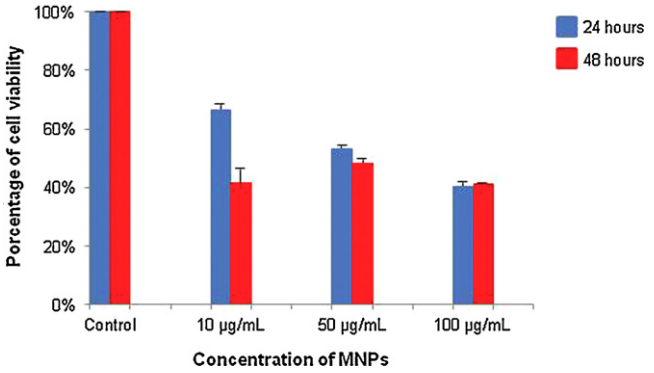

Fig. 6. MTT assay of HeLa cells after 24 and 48 h of incubation with MNP-KOH.

Fig. 5I–O shows the observed results of the apoptotic assay for the HeLa cells incubated with MNP-KOH. It can be noticed that the cells incubated with MNP-KOH at 10 (Fig. 5K and L) and 50 μg/mL (Fig. 5M and N) presented a higher number of live cells, characterized by green nuclei, compared with the cells incubated with MNP-KOH at 100 μg/mL (Fig. 5O).

A detailed analysis of the cells incubated with MNP-KOH at 100 μg/mL revealed a significant color change in the staining of the cytoplasm and the formation of hyperchromatic vesicles. This change can likely be attributed to the increasing cytotoxicity of the cellular environment combined with the high amount of MNPs when cells were incubated with MNP-KOH at 100 μg/mL. These cells also presented typical signs of programmed HeLa cell death, such as cell shrinkage, blebs, and nuclear condensation or fragmentation. Cells in the later stages of apoptosis and secondary necrosis stained in orange–red were also observed.

3.4. MTT assay

The MTT assay for the evaluation of cell viability has been described as a suitable method for the detection of biomaterial toxicity [18]. Nanoparticles have a strong potential to agglomerate, both in air and in liquid solutions, such as the fluid compartments of the body. The potential of the interaction will depend on gravitation, diffusion, convection forces, electrolyte/salt content, cell type, pH and protein composition, either in culture media or in body fluids, and in this aspect, the extent of agglomeration might affect the ability of nanoparticles to interact with cells in in vitro systems [19,20,21].

In this study, the cells incubated with MNP-KOH were evaluated by the MTT assay in parallel with control experiments for two different time intervals: 24 and 48 h. The cells incubated with MNP-NH_4OH and MNP-DABCO exhibited low transfection efficiency; therefore, they were not subjected to the MTT assays.

The cells retained their viability for both 24 and 48 h in the experimental control. The viability of the HeLa cells decreased in conjunction with the increase in the MNP-KOH concentration 24 and 48 h after cell incubation with MNP-KOH. Thus, after 24 h, HeLa cells presented viability higher than 50% when incubated at 10 and 50 μg/mL. After 48 h, HeLa cells presented viability higher than 50% when incubated at 50 μg/mL. In contrast, after 24 and 48 h, HeLa cells incubated with MNP-KOH at 100 μg/mL presented viability lower than 50%, suggesting that this MNP-KOH concentration is the most cytotoxic to HeLa cells (Fig. 6).

When HeLa cells were incubated with the MNP-KOH at 10 μg/mL, there was a continuous decrease in viability in comparison with the control experiment after 24 and 48 h, relating the decrease in the cell population to the toxicity of the nanoparticles. These results are consistent with the study of Lankoff et al. [22] and

it is likely that this decrease occurred because cell death or transient stress is more pronounced in cells exposed to less agglomerated particles than in cells exposed to more agglomerated particles, and we observed a lesser amount of agglomerates in cells incubated with MNP-KOH at 10 compared with cells incubated with MNP-KOH at 50 and 100 μg/mL.

However, when the cells were incubated with MNP-KOH at 50 and 100 μg/mL, the behavior of the cell population was very different from the expected results [16]. We observed a very small difference between the cell populations studied at 24 and 48 h at these MNP-KOH concentrations. Although working with silver nanoparticles, Lankoff et al. have also observed similar behavior with these nanoparticles. Most of their particles had a negative Zeta potential; their sizes were in the range of 20–200 nm [22] and the studies were performed both in water and cell medium. The higher metabolic activity (reduced toxicity) was observed for the nanoparticles incubated with the cell medium, and all of the particles had a negative Zeta potential [22]. We have observed the same behavior (see Fig. 6), and we attempted to explain this behavior as a function of the cell medium.

Lankoff et al. have reported that agglomerated nanoparticles were detected in the cytoplasm, whereas single nanoparticles were detected in the nucleus and mitochondria. Our results also showed the formation of aggregates in the cytoplasm (see Fig. 5E and G), although we were not able to detect the presence of single nanoparticles in the nucleus. From a toxicological point of view, it is important to determine how the agglomeration state of nanoparticles may affect the biological response. It is likely that the intracellular distribution of the nanoparticles could account for the differences in the interaction of these particles with proteins and the DNA inside a cell, followed by different toxic consequences. Xu et al. [23] and Asati et al. [24] have reported that the subcellular localization of nanoparticles plays an important role in the toxicity profile, with lower toxicity when the nanoparticles are localized in the cytoplasm of cells and higher toxicity when the nanoparticles are accumulated in the nuclei and lysosomes [24]. In our study, we observed agglomerates of MNP-KOH in the cytoplasm of the cells, and we suggest that the nanoparticles analyzed in our study have similar characteristics to the nanoparticles analyzed by Lankoff et al. because MNP-KOH nanoparticles also have a negative zeta potential and agglomerate in the cytoplasm of the cells.

We suggest that HeLa cells exhibit a relatively rapid uptake of MNP-KOH nanoparticles because, after 24 h, we have already observed HeLa cells labeled with MNP-KOH, and likely after this period the cells reached the uptake saturation and the amount of nanoparticles taken into the cell did not further increase. HeLa cells presented a lower percentage of viability at 50 and 100 μg/mL MNP-KOH after 24 h of incubation compared with the control and 10 μg/mL MNP-KOH because of the higher level of cytotoxicity at these concentrations, but after 24 h, they reached uptake saturation, and the rate of apoptosis decreased because the MNP-KOH nanoparticles were agglomerated in the cytoplasm and presented low cytotoxicity to these cells. Sirimuthu et al. [14] observed that the amount of metal nanoparticles taken into CHO cells after more than 16 h of incubation did not further increase. They also observed that the CHO cells continued to grow and divide despite having taken up large numbers of nanoparticles.

We supposed that MNP-KOH, which presented a negative Zeta potential and formed agglomerates in the cytoplasm of HeLa cells, were associated with a decreased rate of cell death once the cell reached uptake saturation after 24 h because the amount of agglomerates in the cytoplasm is higher in cells incubated with 50 and 100 μg/mL and is therefore less toxic to cells compared with cells incubated with MNP-KOH at 10 μg/mL, inasmuch as the latter cells exhibit a smaller amount of agglomerates resulting in a higher level of cytotoxicity.

4. Conclusions: possible explanations for the stabilization of the cellular viability

The most relevant finding in this study was that uncoated MNP-KOH at different concentrations (50 and 100 μg/mL) presented a stabilization of the cell viability after 48 h. This result indicates that, after this period of time, the cell population was stabilized. This observation is very surprising, and one possible explanation for this behavior is that the cell medium (DMEM) is able to react with the MNPs and stabilize them, thereby precluding the side reactions to which magnetite particles are subjected. Magnetite nanoparticles are not very stable under ambient conditions and are easily oxidized to maghemite or dissolved in an acidic medium. Because maghemite is a ferrimagnet, oxidation is the lesser problem. Therefore, magnetite particles can be subjected to deliberate oxidation to convert them into maghemite. It is quite possible that maghemite is very toxic to the cells but that, when the magnetite reacts with DMEM, this natural oxidation of magnetite to maghemite is stopped and the cell population is stabilized. These data demonstrate the biocompatibility of MNP-KOH at 50 μg/mL and additional studies could be performed with this nanoparticle to explore possible biomedical applications.

Disclosure statement

All authors must disclose any actual or potential conflict of interest.

Acknowledgements

The study reported in this article is funded by government agencies, such as the São Paulo Science Foundation (FAPESP) grants (05/54703-6 and 09/11203-4), The National Council for Scientific and Technological Development (CNPq) grant (301596/2011-5). Financial support is also provided by a private company (Braile Biomedica Industria, Comercio e Representações Limitada).

References

[1] M. Mahmoudi, K. Azadmanesh, M.A. Shokrgozar, W.S. Journeay, S. Laurent, Effect of nanoparticles on the cell life cycle, Chem. Rev. 111 (2011) 3407–3432.
[2] S. Laurent, D. Forge, M. Port, A. Roch, C. Robic, L.V. Elst, R.N. Muller, Magnetic iron oxide nanoparticles: synthesis, stabilization, vectorization, physicochemical characterizations, and biological applications, Chem. Rev. 108 (2008) 2064–2110.
[3] V. Mailander, M.R. Lorenz, V. Holzapfel, A. Musyanovych, K. Fuchs, M. Wiesneth, P. Walther, K. Landfester, H. Schrezenmeier, Carboxylated superparamagnetic iron oxide particles label cells intracellularly without transfection agents, Mol. Imaging Biol. 10 (2008) 138–146.
[4] K. Montet-Abou, X. Montet, R. Weissleder, L. Josephson, Cell internalization of magnetic nanoparticles using transfection agents, Mol. Imaging 6 (2007) 1–9.
[5] A.S. Arbab, G.T. Yocum, L.B. Wilson, A. Parwana, E.K. Jordan, H. Kalish, J.A. Frank, Comparison of transfection agents in forming complexes with ferumoxides, cell labeling efficiency, and cellular viability, Mol. Imaging 3 (2004) 24–32.
[6] S. Ju, G. Teng, Y. Zhang, M. Ma, F. Chen, Y. Ni, In vitro labeling and MRI of mesenchymal stem cells from human umbilical cord blood, Magn. Reson. Imaging 24 (2006) 611–617.
[7] T. Ishikawa, S. Kataoka, K. Kandori, The influence of carboxylate ions on the growth of beta-feooh particles, J. Mater. Sci. 28 (1993) 2693–2698.
[8] T. Ishikawa, T. Takeda, K. Kandori, Effects of amines on the formation of beta-ferric oxide hydroxide, J. Mater. Sci. 27 (1992) 4531–4535.
[9] K. Kandori, Y. Kawashima, T. Ishikawa, Effects of citrate ions on the formation of monodispersed cubic hematite particles, J. Colloid Interface Sci. 152 (1992) 284–288.
[10] R.H. Daniels, G.T. Kerr, L.D. Rollmann, Cationic polymers as templates in zeolite crystallization, J. Am. Chem. Soc. 100 (1978) 3097–3100.
[11] M. Ivankovic, A. Cukusic, I. Gotic, N. Skrobot, M. Matijasic, D. Polancec, I. Rubelj, Telomerase activity in HeLa cervical carcinoma cell line proliferation, Biogerontology 8 (2007) 163–172.
[12] H. Cui, Y. Feng, W. Ren, T. Zeng, H. Lv, Y. Pan, Strategies of large scale synthesis of monodisperse nanoparticles, Recent Patents Nanotechnol. 3 (2009) 32–41.
[13] R.E. Serda, S. Ferrati, B. Godin, E. Tasciotti, X. Liu, M. Ferrari, Mitotic trafficking of silicon microparticles, Nanoscale 1 (2009) 250–259.

[14] N.M. Sirimuthu, C.D. Syme, J.M. Cooper, Monitoring the uptake and redistribution of metal nanoparticles during cell culture using surface-enhanced Raman scattering spectroscopy, Anal. Chem. 82 (2010) 7369–7373.
[15] V. Mailander, K. Landfester, Interaction of nanoparticles with cells, Biomacromolecules 10 (2009) 2379–2400.
[16] M. Mahmoudi, A. Simchi, M. Imani, M.A. Shokrgozar, A.S. Milani, U.O. Hafeli, P. Stroeve, A new approach for the in vitro identification of the cytotoxicity of superparamagnetic iron oxide nanoparticles, Colloids Surf. B: Biointerfaces 75 (2010) 300–309.
[17] C. Wilhelm, C. Billotey, J. Roger, J.N. Pons, J.C. Bacri, F. Gazeau, Intracellular uptake of anionic superparamagnetic nanoparticles as a function of their surface coating, Biomaterials 24 (2003) 1001–1011.
[18] T. Mosmann, Rapid colorimetric assay for cellular growth and survival: application to proliferation and cytotoxicity assays, J. Immunol. Methods 65 (1983) 55–63.
[19] J.G. Teeguarden, P.M. Hinderliter, G. Orr, B.D. Thrall, J.G. Pounds, Particokinetics in vitro: dosimetry considerations for in vitro nanoparticle toxicity assessments, Toxicol. Sci. 95 (2007) 300–312.
[20] D. Lison, L.C. Thomassen, V. Rabolli, L. Gonzalez, D. Napierska, J.W. Seo, M. Kirsch-Volders, P. Hoet, C.E. Kirschhock, J.A. Martens, Nominal and effective dosimetry of silica nanoparticles in cytotoxicity assays, Toxicol. Sci. 104 (2008) 155–162.
[21] M. Vippola, G.C. Falck, H.K. Lindberg, S. Suhonen, E. Vanhala, H. Norppa, K. Savolainen, A. Tossavainen, T. Tuomi, Preparation of nanoparticle dispersions for in vitro toxicity testing, Human Exp. Toxicol. 28 (2009) 377–385.
[22] A. Lankoff, W.J. Sandberg, A. Wegierek-Ciuk, H. Lisowska, M. Refsnes, B. Sartowska, P.E. Schwarze, S. Meczynska-Wielgosz, M. Wojewodzka, M. Kruszewski, The effect of agglomeration state of silver and titanium dioxide nanoparticles on cellular response of HepG2, A549 and THP-1 cells, Toxicol. Lett. 208 (2012) 197–213.
[23] P.S. Xu, E.A. Van Kirk, Y.H. Zhan, W.J. Murdoch, M. Radosz, Y.Q. Shen, Targeted charge-reversal nanoparticles for nuclear drug delivery, Angew. Chem. Int. Ed. 46 (2007) 4999–5002.
[24] A. Asati, S. Santra, C. Kaittanis, J.M. Perez, Surface-charge-dependent cell localization and cytotoxicity of cerium oxide nanoparticles, ACS Nano 4 (2010) 5321–5331.